International Journal of Pharmaceutics 661 (2024) 124404

Contents lists available at ScienceDirect

International Journal of Pharmaceutics

journal homepage: www.elsevier.com/locate/ijpharm

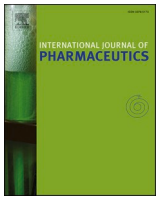

Boosting antigen-specific T cell activation with lipid-stabilized protein nanoaggregates

Michele Schlich [a,b,*], Luciana D'Apice [c], Francesco Lai [a], Chiara Sinico [a], Donatella Valenti [a], Federico Catalano [d], Roberto Marotta [d], Paolo Decuzzi [b], Paola Italiani [c], Anna Maria Fadda [a,*]

[a] Dept. of Life and Environmental Sciences, University of Cagliari, 09124 Cagliari Italy
[b] Laboratory of Nanotechnology for Precision Medicine, Istituto Italiano di Tecnologia, 16163 Genoa Italy
[c] National Research Council (CNR) - Institute of Biochemistry and Cell Biology (IBBC), 80131 Naples Italy
[d] Electron Microscopy Facility, Fondazione Istituto Italiano di Tecnologia, 16163 Genoa Italy

ARTICLE INFO

Keywords:
Microfluidics
Ovalbumin
Vaccines
Nanoaggregates
Purified antigens

ABSTRACT

Vaccines based on protein antigens have numerous advantages over inactivated pathogens, including easier manufacturing and improved safety. However, purified antigens are weakly immunogenic, as they lack the spatial organization and the associated 'danger signals' of the pathogen. Formulating vaccines as nanoparticles enhances the recognition by antigen presenting cells, boosting the cell-mediated immune response. This study describes a nano-precipitation method to obtain stable protein nanoaggregates with uniform size distribution without using covalent cross-linkers. Nanoaggregates were formed via microfluidic mixing of ovalbumin (OVA) and lipids in the presence of high methanol concentrations. A purification protocol was set up to separate the nanoaggregates from OVA and liposomes, obtained as byproducts of the mixing. The nanoaggregates were characterized in terms of morphology, ζ-potential and protein content, and their interaction with immune cells was assessed *in vitro*. Antigen-specific T cell activation was over 6-fold higher for nanoaggregates compared to OVA, due in part to the enhanced uptake by immune cells. Lastly, a two-dose immunization with nanoaggregates in mice induced a significant increase in OVA-specific $CD8^+$ T splenocytes compared to soluble OVA. Overall, this work presents for the first time the microfluidic production of lipid-stabilized protein nanoaggregates and provides a proof-of-concept of their potential for vaccination.

1. Introduction

The development of vaccines and their deployment in large immunization programs reduced mortality and severity of infectious diseases, in some cases leading to the global eradication of deadly pathogens (Pollard and Bijker, 2020). Vaccines induce an adaptive immune response that protects the individual from the infection upon subsequent exposure through the production of antibodies and the activity of T cells. While numerous vaccines are known to induce robust antibody responses, their effect on the establishment of a cellular immunity has often been overlooked (Seder et al., 2008; Walls et al., 2020). In fact, if rapid production of neutralizing antibodies is thought to have a role in disease prevention, cellular immune response is required to fight off an existing infection, especially if this is triggered by intracellular pathogens such as HIV (Collins et al., 2020). The ability to trigger a potent T cell activation is an essential requirement also for cancer vaccines, where the magnitude of neoantigen-specific T cell response has been correlated with better outcomes in clinical trials (Blass and Ott, 2021). T cell response is a complex and well-orchestrated process that include $CD8^+$ and $CD4^+$ cells proliferation, secretion of growth factor to induce other cells' proliferation, production of chemokines and cytokines, and direct killing of infected/tumoral cells (Seder et al., 2008). The quality of T cell response depends on different properties of the antigen, including immunogenicity, stability and uptake by antigen presenting cells (APCs). Professional APCs endocytose the foreign antigen, process it into peptide epitopes, and present them on major histocompatibility complexes (MHC-I and MHC-II) to prime $CD8^+$ and $CD4^+$ cells, respectively, in a process called cross presentation. Strategies aimed at promoting the efficacy of cross presentation by enhancing antigen uptake and modulating intracellular trafficking are actively researched to enhance T cell response and, ultimately, vaccination efficacy (Foged et al., 2012; Urbanavicius et al., 2018). Nanoparticles of different nature

* Corresponding authors at: Dept. of Life and Environmental Sciences, University of Cagliari, 09124 Cagliari Italy.
E-mail addresses: michele.schlich@unica.it (M. Schlich), mfadda@unica.it (A. Maria Fadda).

https://doi.org/10.1016/j.ijpharm.2024.124404
Received 6 May 2024; Received in revised form 26 June 2024; Accepted 27 June 2024
Available online 28 June 2024

have been developed with the specific aim of improving the delivery of antigens to APCs, sometimes with the additional benefit of stimulating a mild inflammation to enhance the immune response (Gao et al., 2017; Pedersen et al., 2018; Sartorius et al., 2018). The nanotechnology approach proved to be particularly useful in the case of highly purified protein/peptidic antigens. Protein antigens (also called subunit vaccines) have several advantages in terms of ease of production, characterization and safety compared to inactivated pathogens, but they are known to be scarcely immunogenic if not properly formulated (e.g., supplemented with adjuvants). Nanoparticles can improve the performance of subunit vaccines by enhancing their stability against premature degradation, promoting their cytosolic localization and improving the delivery to lymph nodes (Carson et al., 2022; Kapadia et al., 2016; Pati et al., 2018; Schmidt et al., 2016). Moreover, the spatial organization of antigens on the surface of nanoparticles can boost their immunogenicity by mimicking the size and shape of pathogens (Nguyen and Tolia, 2021). In general, surface-exposed arrays of antigens can be generated by chemical conjugation to nanoparticles (Shimp et al., 2013) or peptides (Jiang et al., 2020), by genetic engineering of the protein (Tian et al., 2021), or by inducing antigen aggregation through crosslinking (Dong et al., 2018) or stress-induced denaturation (Ahmad et al., 2017; White et al., 2008). Protein aggregates are known to be more immunogenic than soluble proteins, as they are more avidly endocytosed by APCs, they stimulate B and T cells and prolong the release of antigens (Wang et al., 2012). As such, while aggregates are an undesirable issue for biopharmaceuticals in general, they might represent an opportunity in the field of vaccine formulation (Snapper, 2018). For instance, immunization of mice with fibrillar aggregates of the mycobacterium antigen Ag85B led to enhanced T-cell expansion and activation compared to the soluble antigen, outperforming the standard Bacillus Calmette-Guerin (Ahmad et al., 2017). In a previous report, the aggregated fraction of five different heat-denatured proteins consistently led to antigen-specific cytotoxic T cell responses, that were not observed when injecting the corresponding soluble fraction (Speidel et al., 1997). Protein denaturation is often the trigger for the formation of aggregates. If on one hand this could lead to a reduction in the humoral response due to changes in the protein higher order structure, the potentiation of the T-cell response could be worth such reduction, especially in the cases when the cellular immunity plays a primary role. In the present work, we produced nanoaggregates (NAG) of the model antigen ovalbumin (OVA) exploiting the tendency of proteins to aggregate upon dilution with an anti-solvent (methanol). Compared to the other nanoparticles used for vaccination discussed above, the production of NAG does not require chemical crosslinking nor genetic engineering, allowing to obtain protein nanostructures through a straightforward and inexpensive procedure. To gain control over the process of aggregation, microfluidic mixing was employed to finely manage solvent and anti-solvent streams (Webb et al., 2020), allowing to obtain stable NAG with uniform size distribution and high protein loading. NAG showed enhanced uptake by APCs and improved $CD8^+$ cell-activating properties compared to soluble OVA both *in vitro* and *in vivo*, proving that microfluidic-controlled protein aggregation can be a quick and scalable method to produce antigen aggregates as vaccination platforms.

2. Materials and methods

2.1. Materials

Distearoylphosphatidylcholine (DSPC), cholesterol, dimethyldioctadecylmmonium bromide (DDAB), ovalbumin (Grade V), fluorescein isothiocyanate (FITC) were purchased from Merck KGaA (Darmstadt, Germany). All other solvents and reagents were purchased from Merck and used without further purification, unless specified. Rabbit polyclonal antibody to Ovalbumin (ab181688) was obtained from Abcam (Cambridge, UK). Gold conjugated anti-rabbit antibody (GAR) is a goat anti-rabbit IgG-gold conjugate (H&L), EM-grade, 10-nm particle size and was obtained from Electron Microscopy Sciences (Hatfield, PA, USA).

2.2. Measurement of the aggregation index

The aggregation index (AI) of ovalbumin was measured in different PBS/methanol mixtures adapting a published protocol (Hawe et al., 2009). Briefly, OVA solubilized in PBS was diluted with MeOH to achieve the desired % of solvent. The mixture was vortexed and transferred to a 96 well plate for absorbance measurements performed at 280 nm and 360 nm. AI was determined using the formula AI = A360/(A280-A360) and values were normalized to the AI of a solution of OVA in PBS (0 % MeOH).

2.3. Production of nanoparticles

Mixtures of DPPC, cholesterol and DDAB were dissolved in methanol at total lipid concentration of 10 mg/ml (unless otherwise stated), using five different lipid compositions (defined in Table 1). A solution of OVA (0.625 mg/ml) was prepared in PBS pH7.4. One volume of lipids in methanol was rapidly mixed with one volume of OVA in PBS using a Nanoassemblr Benchtop (Precision Nanosystems, Vancouver, Canada). The microfluidic mixing led to the formation of a mixed sample containing NAG, liposomes and soluble OVA named hereafter as "LipoNAG" (Fig. 1**D**). The organic solvent was removed dialyzing the sample against a 500x volume of PBS using Pur-A-Lyzer™ Maxi Dialysis cups (MWCO 3.5 kDa) (Merck KGaA). The same procedure was carried out to produce fluorescently labelled nanoparticles, replacing OVA with a FITC-OVA conjugate synthesized as previously reported with slight modifications.(Könnings et al., 2002) Briefly, 1.25 mg FITC in DMSO were added to 50 mg OVA solubilized in 5 ml carbonate buffer (pH 9.0) and allowed to react overnight in the dark. The conjugate was extensively dialyzed against water, replacing the dialysis medium until its fluorescence intensity was not significantly different from a blank, then freeze-dried and stored at 4 °C.

2.4. Separation of NAG from soluble OVA and liposomes

LipoNAG were fractionated in its components (NAG, liposomes, and soluble OVA) by centrifugation. LipoNAG were centrifuged at 4 °C, 13,000 RPM for 90 min. The supernatant containing liposomes and soluble OVA was separated from the pellet containing NAGs. NAGs were resuspended in PBS and used for all the characterizations, as well as for *in vitro* and *in vivo* studies.

2.5. Dimensional and morphological analysis

Size, polydispersity index (PDI) and ζ-potential of LipoNAG and isolated NAG were determined using a Zetasizer Nano ZS (Malvern Panalytical Ltd, Worcestershire, UK) equipped with a 633 nm laser and a detection angle of 173°. The co-existence of liposomes and NAG in the LipoNAG sample, as well as the morphology of the two populations of nanoparticles, were observed by cryo-transmission electron microscopy (cryo-EM). The sample was vitrified in liquid ethane cooled at liquid nitrogen temperature using a FEI Vitrobot Mark IV semiautomatic autoplunger. Bright field cryo-EM was run at − 176 °C in a FEI Tecnai G2 F20 transmission electron microscope, working at an acceleration

Table 1
Composition of lipid mixtures expressed as weight ratios.

Sample ID	0 %	1 %	5 %	10 %	20 %
DDAB	0	1	5	10	20
Cholesterol	32	32	32	32	32
DPPC	68	67	63	58	48

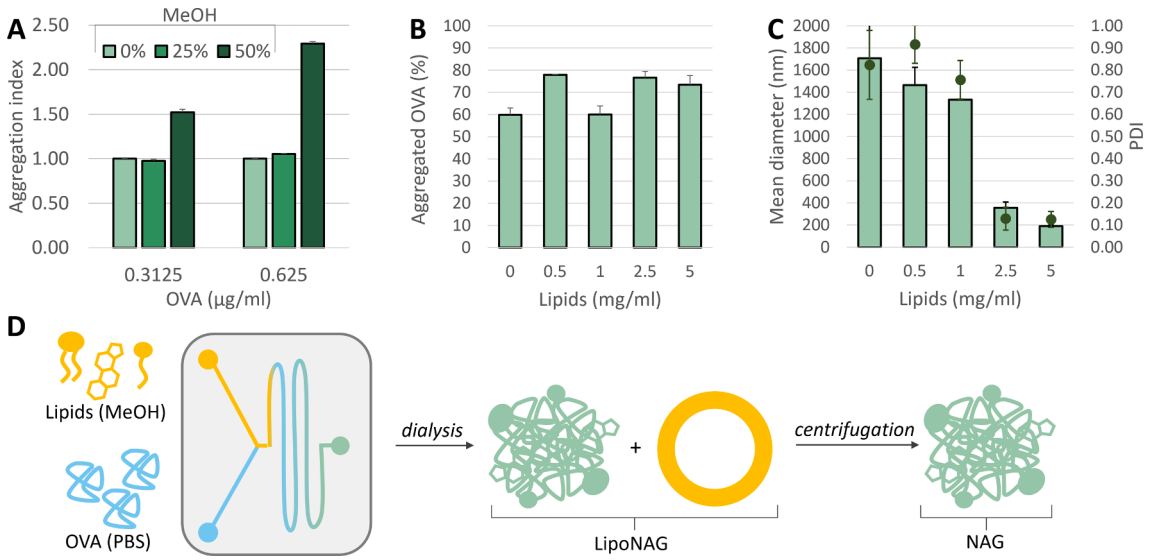

Fig. 1. Aggregation index of OVA measured in different PBS/methanol mixtures (n = 3) (**A**). Amount of OVA in aggregates prepared using different concentrations of lipids (100 % = OVA input) (n = 3) (**B**). Mean diameter (full bars) and PdI (dots) of LipoNAG prepared using different concentrations of lipids (n = 3) (**C**). Schematic representation of the production and purification of NAG: lipids in methanol are rapidly mixed with OVA in PBS in a staggered herringbone micromixer. The organic solvent is removed by dialysis and a mixed sample containing NAG and liposomes is obtained (LipoNAG). NAGs are separated from liposomes and soluble OVA through centrifugation (**D**).

voltage of 200 kV and equipped, relevant for this project, with a field emission gun and automatic cryo-box. The images were acquired in a low dose modality with a GATAN Ultrascan 1000 2 k × 2 k CCD.

2.6. Immuno electron microscopy

A 5 µl drop of LipoNAG was deposited on plasma-cleaned carbon coated Cu grids 150 mesh (Electron Microscopy Sciences, Hatfield, PA, USA) and adsorbed for 2 mins. After two washing steps with 50 µL of phosphate buffered saline (PBS) (Sigma-Aldrich, St. Louis, MO, USA), sample was incubated with 50 µL of rabbit anti-OVA pAb (8 µg/mL) and allowed to react with the sample for 30 mins in a wet chamber. After washing with PBS to remove the unreacted antibody, the grid was treated for 30 min with the secondary Goat anti-rabbit Ab conjugated with 10-nm Au particles (AuNP, 1:40 dilutions in PBS). Following a second washing step with PBS, the sample was washed several times with distilled water and negatively stained with 1 % uranyl acetate in water. A control sample was prepared in the same way, substituting the primary anti-OVA pAb with a solution of 1 % BSA in PBS. Samples were imaged by a JEM-1011 (JEOL) transmission electron microscope (TEM) with a thermionic source (W filament) and maximum acceleration voltage of 100 kV equipped with a Gatan OriusSC1000 series CCD camera (4008 × 2672 active pixels). Statistical analysis was carried out on two replicates for each sample, counting the number of NAG and AuNP in a 40 μm^2 area and calculating the percentage of AuNP bound to NAG (Au linked %), and the percentage of NAG labeled by at least one AuNP (Marked NAG %).

2.7. OVA quantification

OVA was quantified using a Quantum Protein BCA kit (Euroclone). Briefly, the samples obtained from the separation procedures (described in paragraph 2.3) were treated with an SDS/TritonX mixture (1 % and 0.5 % w/w, respectively) to solubilize the nanoparticles. The lysed samples were then incubated with the BCA working solution following the manufacturer's protocol. Absorbance was measured at 562 nm using a microplate reader (Tecan, CH), and OVA amounts calculated according to a calibration curve built using OVA standard solutions diluted in the same buffer of the samples.

2.8. Cytotoxicity studies

The murine macrophage cell line RAW 264.7 was obtained by the American Type Culture Collection (ATCC) and cultured in Dulbecco's Modified Eagle Medium (DMEM) supplemented with 10 % Fetal Bovine Serum (FBS), 1 % penicillin/streptomycin and L-glutamine. For the experiments described in this work, cells at passage number between 15 and 32 were employed. Cells were kept in a humidified incubator with 5 % CO_2 and at 37 °C and sub-cultured as advised by the supplier. For cytotoxicity studies, cells were seeded in 96 well plates (10^4 cells/well) and allowed to attach and grow for 24 h. NAG or LipoNAG were diluted in complete medium and added on cells at OVA concentrations of 3.91——62.5 µg/ml. The toxicity of soluble OVA at the same concentrations was tested for comparison. After 24 h the treatments were replaced with medium containing (3-(4,5-dimethylthiazolyl)-2,5-diphenylte- trazolium bromide (MTT) (0.25 mg/ml), left in contact with the cells for 3 h. The formazan crystals formed were then dissolved in ethanol (200 µL/well) and the 570 nm absorbance was read by a microplate reader (Tecan, CH).

2.9. Cell internalization

For cell internalization studies, the fluorescently labelled FITC-OVA was employed to prepare NAG, as described in paragraph 2.2. RAW 264.7 cells were seeded in 96 well plates ($4x10^4$ cells/well) and allowed to attach. After 24 h, NAGs were added to the wells at FITC-OVA concentrations of 1.25——31.25 µ g/ml. After 4 h, cells were washed with PBS and lysed with a solution of TritonX/SDS. The fluorescence intensity of the lysis solution was measured at excitation/emission wavelengths of 488/520 nm using a microplate reader. Cell uptake was also visualized by confocal laser scanning microscopy (CLSM), using the following protocol. RAW 264.7 cells were plated in µ-Slide 8 well plates (ibiTreat, Ibidi) at a density of $4x10^4$ cells/well. After 24 h, NAGs were added to the wells at FITC-OVA concentrations of 1.25——6.25 µ g/ml and allowed to interact with cells for 4 h. Cells were then washed extensively with PBS, fixed with PFA 4 % and stained with Wheat Germ Agglutinin (WGA)-AlexaFluor™ 647-conjugate (ThermoFischer) and DAPI to mark membranes and nuclei, respectively. Cells were observed under a Nikon A1plus CLSM using a Plan Apo λ 60x Oil optic.

2.10. Human monocytes isolation and activation

Human monocytes were obtained from buffy coat of healthy donors (n = 2) by gradient density centrifugation with Ficoll-Paque PLUS (GE Halthcare, Bio-Sciences AB, Uppsala, Sweden), and isolation using CD14 positive selection with magnetic microbeads (Miltenyi Biotec, Bergisch Gladbach, Germany). All samples of human blood included in this study were obtained from anonymous volunteers after informed consent, and all were donated by hospital "Azienda Ospedaliera Universitaria Federico II" as discarded blood products. Monocytes were cultured in culture medium (RPMI 1640 + Glutamax-I; GIBCO by Life Technologies, Paisley, UK) supplemented with 50 μg/mL gentamicin sulfate (GIBCO) and 5 % heat-inactivated human AB serum (Merck Sigma-Aldrich®). Cells (5×10^5) were seeded at a final volume of 1.0 mL/well in 24-well flat bottom plate (Corning® Costar®; Corning Inc. Life Sciences, Oneonta, NY, USA) at 37 °C in moist air with 5 % CO2. After resting overnight, monocytes were exposed for 24 h to culture medium alone (negative control) or medium containing 5 ng/mL LPS (positive control; from E. coli O55:B5; Merck Sigma-Aldrich®), and to liposomes alone or LipoNAG or NAG loaded with two different concentration of OVA (0.2 and 1 μg/ml) and prepared with different percentage of cationic surfactant DDAB. All supernatants were frozen at − 20 °C for subsequent cytokine analysis. The levels of the inflammatory cytokines TNFα and IL-6 were assessed by ELISA (R&D Systems, Minneapolis, MN, USA) according to manufacturers' instructions. Each sample was tested in duplicate.

2.11. Ova-specific T cell immune response in vitro

All animal experiments were carried out in accordance with the European Community guidelines (directive 2010/63) and under the approval of the Italian Ministry of Health (authorization 551/2020-PR). Bone marrow derived dendritic cells (BM-DCs) were obtained from 8 to 10-week-old C57Bl/6 female mice (Charles River, Lecco, Italy) and housed in IGB "A. Buzzati- Traverso" Animal House Facility under standard pathogen-free conditions in compliance with institutional guidelines. BM-DCs were obtained from precursors isolated from tibiae: both ends of tibiae were cut and the bone marrow was flushed with ice-cold RPMI 1640 medium. Cells clusters were dissolved by pipetting, and cells were washed twice with medium, plated and cultured for 7 days with RPMI 1640 medium supplemented with 200 U/mL recombinant murine granulocyte/macrophage colony-stimulating factor (GM-CSF, Peprotech, NJ, USA), 10 % fetal calf serum (FCS), 60 μg/ml penicillin, 100 μg/ml streptomycin, 1 mM sodium pyruvate and 50 μM 2-mercaptoethanol. Immature DCs were used in the antigen presentation assay: cells (100,000/well) were incubated overnight with antigens (1–5 μg/mL) in 96 well plates. After 21 h, the $OVA_{(257\text{-}264)}$ specific B3Z cells (50,000/well) were added to the culture and incubated for further 40 h. At the end of the experiment, cell culture medium was collected and IL-2 secreted in the supernatants was measured by ELISA(0.1 ml/well in duplicate) using mouse IL-2 ELISA MAX Standard (Biolegend, San Diego, CA), according to the manufacturer's instructions. Results are representative of two independent experiments.

B3Z hybridoma cells, recognizing the $OVA_{(257–264)}$ SIINFEKL determinant, were grown in complete RPMI1640 (10 % FCS, 100 U/ml penicillin, 100 μg/ml streptomycin 1 % Glutamine, 1 % NEM, 1 % Sodium Pyruvate, 50 μM 2-Mercaptoethanol).

2.12. In vivo analysis of immune response

Mice (C57Bl/6, female, n = 3/6) were immunized with subcutaneous injection at day 0 and day 14 with indicated compounds (2.27 mg_{OVA}/kg), previously sterilized by UVC radiation. Alum was used as adjuvant at the alum:antigen ratio of 1:1.86. At day 21 blood was collected by retroorbital bleeding, mice were sacrificed, and spleens were harvested. Spleens were passed through cell strainers, red cells were lysed by incubation with red blood cell lysis buffer (Sigma) and splenocytes were collected, counted, and stained with APC-anti CD3, FITC-anti CD8 antibodies (Biolegend) and H-2 Kb/ SIINFEKL/PE dextramers (Immudex) according to manufactures' instructions. After washing, cells were analyzed by FACSCanto II (BD) and BD Diva software.

2.13. Statistical analysis

Data were processed using Excel (Microsoft). Results are expressed as mean ± standard deviation (SD). One-way ANOVA and Tukey's multiple comparison test was performed to substantiate statistical differences between groups, while Student's *t*-test was used to compare two samples.

3. Results and discussion

3.1. Nanoprecipitation of ovalbumin and stabilization by lipids

OVA is a 44.5 kDa monomeric globular protein with isoelectric point of 4.5 (Rupa and Mine, 2011). Like numerous other proteins, OVA is not soluble in alcoholic solvents, that induce its precipitation by dehydration and consequent aggregation due to van der Waals forces (van Oss, 1989). Initially, we identified the minimum amount of methanol (antisolvent) required to induce the precipitation of OVA from a PBS solution by measuring its aggregation index in PBS/MeOH mixtures. The aggregation index can be quickly determined by UV spectroscopy, as protein aggregates scatter incident light, showing an apparent absorption at 360 nm (that is not produced by soluble proteins). Here, the aggregation index indicates the relative aggregation of OVA, allowing for comparisons between different solvent mixtures. At the concentration of 0.625 mg/ml, the aggregation indexes of OVA in PBS and in PBS/MeOH (75:25, v/v) was not significantly different, while a PBS/MeOH mixture (50:50, v/v) led to a visible precipitation and higher aggregation index (Fig. 1**A**). From this preliminary experiment, we decided to proceed with a solvent/antisolvent ratio of 1:1 to induce the precipitation of OVA. To control the process with greater accuracy, we employed a microfluidic platform and finely regulated the mixing of OVA in buffer and methanol. Using a Nanoassemblr Benchtop, one volume of OVA in PBS was rapidly mixed with one volume of methanol, and the product dialyzed against PBS to remove the organic solvent. The so formed aggregates were collected by centrifugation and analyzed for protein content and hydrodynamic diameter. In these conditions, 60 ± 3 % of the initial OVA input was recovered as aggregates (Fig. 1**B**). However, such aggregates are characterized by a large size (>1,000 nm) and high polydispersity (>0.6) (Fig. 1**C**), suggesting that the controlled mixing between the solvent and the antisolvent is not sufficient to induce the nano-precipitation of size-defined particles. The removal of methanol during the dialysis could be one of the causes of such polydispersity, as the desolvation of lipophilic portions on different protein particles promotes the aggregation. A similar tendency towards irreversible flocculation was previously reported for pure protein particles produced by a dense gas method, where eventually the authors stabilized OVA particles at pH suitable for injections by adding Pluronic F127 to the formulation (White et al., 2012).

Here, in order to stabilize OVA aggregates after nano-precipitation, a mixture of lipids (composition detailed in Table 1**, 20** %) was included in the antisolvent stream during the microfluidic mixing, varying the final concentration between 0.5 and 5 mg/ml (Fig. 1**D**). The presence of lipids and their concentration did not affect the mass of precipitated OVA, that was always ranging between ~ 60 and 80 % of the input (Fig. 1**B**). On the other hand, lipid concentration higher than 2.5 mg/ml led to the formation of nanoparticles with smaller diameter and narrower size distribution (Fig. 1**C**). This observation suggests that lipids have a concentration-dependent role in the stabilization of nascent protein aggregates and prevention of particle growth, probably occupying the hydrophobic pockets of denatured proteins with their lipophilic portions

and exposing the hydrophilic heads towards the solvent. OVA nanoparticles for further experiments were thus produced by microfluidic antisolvent precipitation and stabilized by lipids at a total concentration of 5 mg/ml.

3.2. Characterization of the morphology and composition of nanoparticles

To elucidate the structure and properties of nanoparticles, a thorough physico-chemical characterization was carried out. First, the samples obtained after microfluidic mixing and dialysis were imaged by cryo-TEM to allow their observation in the hydrated state. As visible in Fig. 2**A** and Fig. 2**B**, electron-dense, spherical nanoparticles with ragged edges could be detected and identified as nanoaggregates (NAG). NAGs were surrounded by numerous uni/oligolamellar lipid vesicles. This complex sample containing NAG and liposomes was named LipoNAG. The presence of liposomes can be easily explained if one considers the production method and the materials employed, as microfluidic mixing of lipids in alcohols with a buffer is conventionally used to produce liposomes (Khadke et al., 2019). In our process, along the microfluidic channel a portion of lipids was recruited to stabilize the protein nanoaggregates precipitating due to the increasing amount of methanol, while another portion self-assembled into vesicular structures to minimize the contact of hydrophobic tails with the increasing amount of water, leading to the formation of two populations of nanostructures. The recruitment of lipids on protein nanoaggregates was confirmed by LC-MS analysis of purified NAG (**Supporting** Figure 1). Negative-staining TEM was employed as a more accessible and time-efficient technique to investigate the properties of LipoNAG. Fig. 2**C** is a representative negative staining TEM image of LipoNAG, and it is possible to observe round-shaped electron dense particles with size comparable to the one observed via cryo-TEM (green arrows). As a negative control, we also imaged empty liposomes (i.e., produced using the same conditions of LipoNAG without OVA in the aqueous phase) following the same sample preparation and imaging technique (Fig. 2**D**). The absence of the round electron-dense structures in the negative control convinced us that negative staining TEM is suitable to evidence the presence and monitor the size of NAG.

The negative staining TEM analysis was also preparatory to a subsequent characterization aimed at identifying the position of OVA in the sample. More specifically, having a mixed sample with liposomes and NAG, we wanted to clarify whether OVA was prevalently organized as NAG or entrapped in liposomes. To answer this question, a negative staining immuno-TEM was performed on LipoNAG, using a primary polyclonal antibody against OVA and a secondary gold nanoparticle (AuNP)-conjugated mAb to localize the protein in the sample. As visible from Fig. 3**A**, AuNPs clustered around the electron-dense structures previously identified as NAG (green arrows). The specificity of the gold-conjugated secondary mAb was confirmed by imaging a control sample, where the treatment with primary anti-OVA pAb was not performed (Fig. 3**B**). Here, AuNPs appear randomly scattered in the TEM grid, without a defined localization due to unspecific binding. Image analysis allowed us to obtain quantitative data from this experiment, that are reported in Fig. 3**C**. Overall, 94 % of NAG present in the sample were

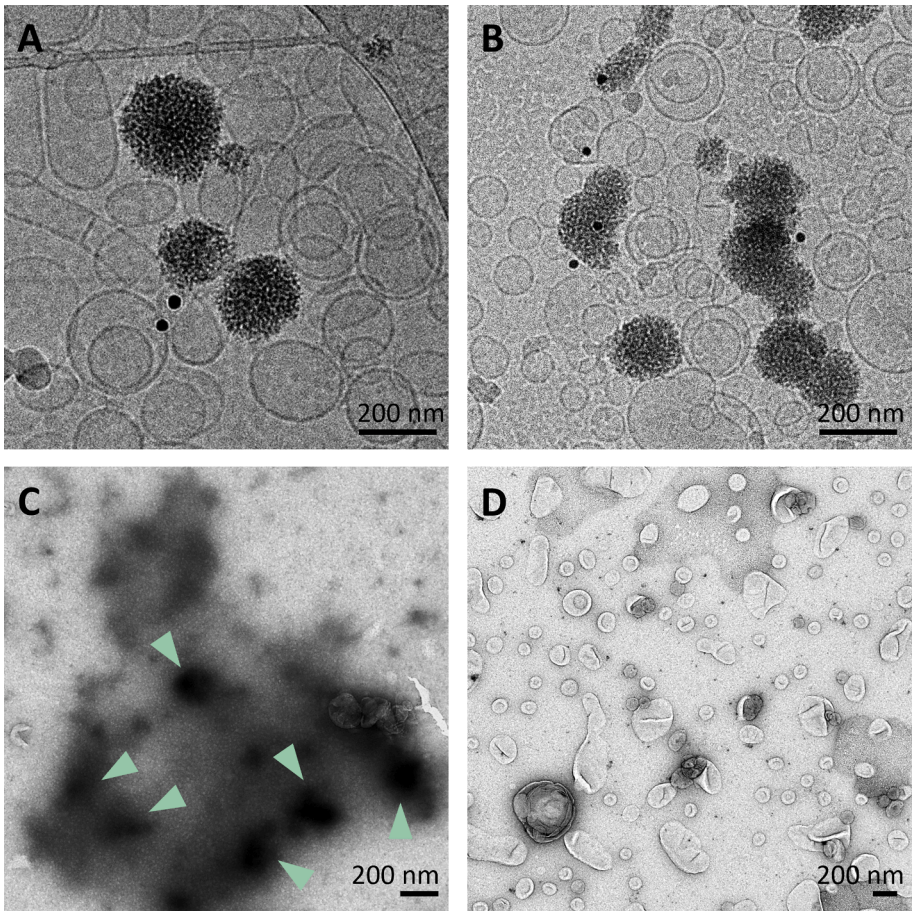

Fig. 2. Representative Cryo-TEM of LipoNAG, showing electron-dense NAGs surrounded by uni/oligolamellar liposomes (two different fields of the same sample). The small black dots are size-defined gold nanoparticles, added before sample vitrification and to be used as a dimensional standard (**A, B**). Representative negative staining TEM of LipoNAG. Green arrowheads highlight electron-dense structures identified as NAGs (**C**). Representative negative-staining TEM of empty liposomes (i.e., prepared in the same conditions of LipoNAG without OVA). Note the absence of electron-dense structures and the presence of lipid vesicles (**D**).

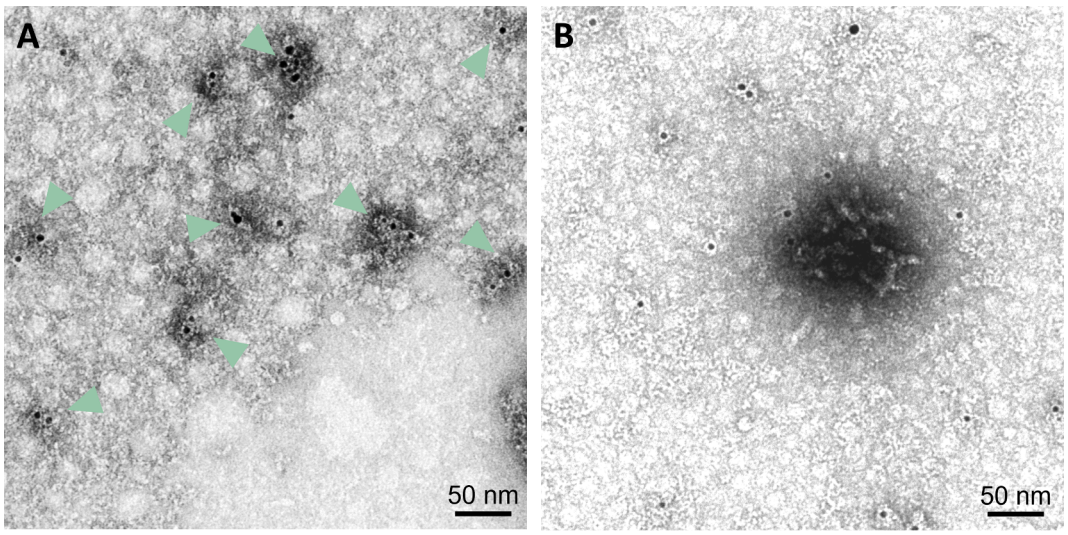

C	#Au/μm²	Au linked (%)	Marked NAG (%)
Anti-OVA pAb	37	56	94
Control	53	11	22

Fig. 3. Representative negative staining immuno TEM of LipoNAG. Green arrowheads highlight electron-dense structures, surrounded by AuNP due to the specific interaction between anti-OVA primary pAb and Au-conjugated secondary antibody (**A**). Control sample, where LipoNAG were treated with PBS instead of the anti-OVA primary pAb. Note the scattered and unspecific distribution of AuNP (**B**). Statistical analysis of AuNP distribution in the LipoNAG samples (anti-OVA pAb-treated VS control) (**C**). #Au/μm^2: number of gold nanoparticles per square micrometer; Au linked (%): percentage of gold nanoparticles linked to NAG in the sample; Marked NAG (%): percentage of NAG in the sample linked to at least one gold nanoparticle.

marked by AuNPs due to the immunoaffinity of the anti-OVA pAb, strongly suggesting that NAGs are composed of OVA. This conclusion is reinforced by the comparison with the control sample, where only 22 % of NAG are marked by gold nanoparticles, despite a higher density of gold was present. Immuno-TEM analysis was crucial to investigate the nature of NAG, a nanostructure that was not reported in previous studies on OVA delivery. Indeed, different groups described the encapsulation of OVA in liposomes as a delivery strategy for antigen vaccines, where such liposomes were prepared through the conventional lipid film hydration (Kim et al., 2022; Wang et al., 2014), or by microfluidic mixing (Forbes et al., 2019; Tabassum et al., 2020). However, works focused on microfluidic mixing as a production technique seldom explore the process parameters reported in the present work (i.e., FRR 1:1), identified by us as critical for the formation of NAG.

3.3. NAG isolation and formulation screening

Having identified LipoNAG as a mixture of two types of nanoparticles (NAG and liposomes) we set up a centrifugation protocol to separate the two fractions. NAG could be isolated as a pellet following high speed centrifugation of LipoNAG, while liposomes remained in the supernatant. The purification protocol was validated employing a complementary test described in the Supplementary Information (**Supporting** Figure 2). The NAG pellet was easily redispersed in buffer and used for further characterization and *in vitro/in vivo* experiments. Upon optimization of the production and isolation protocols using a defined lipid mixture (DDAB 20 %, cholesterol 32 %, DPPC 48 %, w/w) we explored other compositions varying the amount of the cationic lipid DDAB (Table 1) while keeping constant the total lipid concentration (5 mg/ml). Fig. 4**A** reports the results of size and size distribution analyses of NAG produced using different percentages of DDAB, as well as of the LipoNAG mixture from which they were isolated. A trend towards a smaller hydrodynamic diameter at lower DDAB amounts could be observed, while PDI seems to follow an inverse tendency, with a narrower size distribution at higher DDAB amounts. Not surprisingly, size and PDI of LipoNAG derive from the contribution of NAG and liposomes,

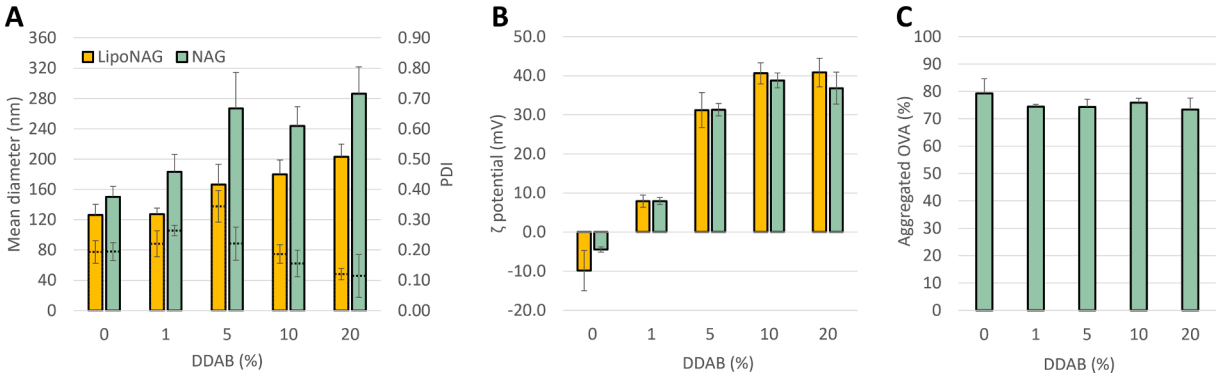

Fig. 4. Mean diameter (full bars) and PdI (dotted lines) of LipoNAG and purified NAG prepared using lipid mixtures with different amounts of the cationic surfactant DDAB (n = 5) (**A**). ζ potential of LipoNAG and purified NAG (n = 3) (**B**). Amount of OVA in NAG, expressed as the percentage of initial OVA input (n = 4) (**C**).

the latter having a basically constant mean diameter of 125 ± 25 nm and PDI < 0.1 regardless of DDAB concentration. ζ-potential values also followed an expected trend, with a more marked cationic charge derived from the higher concentration of DDAB (Fig. 4**B**). Lastly, the tendency of OVA to precipitate and form NAG was not influenced by the amount of cationic lipid in the formulation, as only slight variations in the percentage of aggregated OVA were found between the different compositions (Fig. 4**C**). Overall, all the developed formulations had a narrow size distribution and high OVA content, thus being suitable for an activity and toxicity screening *in vitro*.

3.4. NAG interactions with immune cells in vitro

Imparting a positive charge to nanoparticles enhances the immunostimulatory properties of the vaccine through several mechanism, such as promoting the uptake by macrophages, prolonging the retention at the injection site and triggering a mild inflammation with additional recruitment of peripheral APCs (Chatzikleanthous et al., 2020; Ma et al., 2011; Varypataki et al., 2016). On the other hand, cationic nanoparticles are known to the nanomedicine community for their higher risks, including nonspecific uptake and cell toxicity triggered by perturbation of numerous pathways (Knudsen et al., 2015; Wei et al., 2015). To identify the formulation with the best balance between toxicity and efficacy, the complete panel of NAG with different cationic charge was tested *in vitro*. Initially, a murine macrophage cell line was employed to screen the cytotoxicity of NAG, determined as the effect on the metabolic activity upon 24 h incubation. As expected, formulations with a higher percentage of DDAB had a stronger impact on cell viability, while the effect of NAG prepared with DDAB 0 %, 1 % or 5 % did not differ significantly from the one of soluble OVA at matching concentrations (**Supporting Figure 3A**). The same test was also performed on the unpurified formulations (LipoNAG), revealing that the removal of unnecessary positively charged liposomes during NAG isolation was an important step to improve the biocompatibility (**Supporting** Figure 3**B**). We then moved to primary human monocytes from healthy human donors as a more clinically relevant model to assess the effect of NAG on the production of immunostimulatory/inflammatory cytokines (i.e., TNFα and IL-6). Triggering a mild inflammation might be a desirable feature in the context of vaccination, as it would recruit additional immune cells and support the generation of the adaptive response (Van Duin et al., 2006). Surprisingly, none of the NAG elicited any significant change in TNFα and IL-6 production, a result comparable to the effect of soluble OVA (**Supporting** Figure 4). The unresponsiveness of human monocytes upon exposure to NAG can be explained by the fact that these cells do not perceive NAG, or they are detected but not recognized as dangerous and therefore monocytes do not trigger any reaction. However, further research −including varying the exposure time and concentration- is needed to fully exclude the capacity of NAG to activate the innate immunity.

Next, we investigated the ability of NAG to deliver OVA to murine BMDC, and the efficacy of antigen presentation by measuring the antigen-specific T cell response *in vitro*. OVA, once engulfed by BMDC should be processed and presented to activate T cell response. Recognition of the major histocompatibility complex (MHC-I) loaded with the $OVA_{(257–264)}$ peptide (SIINFEKL) by B3Z T cell receptor lead to the transcriptional activation of the IL-2 promoter element, resulting in production and release of IL-2, which concentration correlates with the uptake and processing of the OVA protein. While all NAG formulations elicited some level of IL-2 production, also in this case the amount of cationic lipid correlated with the intensity of T cell response (Fig. 5). The most efficient formulations in this regard were NAG 10 % and NAG 20 %, that showed 8-fold and 6-fold higher T cell responses compared to soluble OVA, used as control, respectively. It is important to note, however, that the cell responses to treatments with NAG10% and NAG20% were not significantly different. Interestingly, responses to NAG 5 %, 10 % and 20 % were slightly reduced when higher doses of

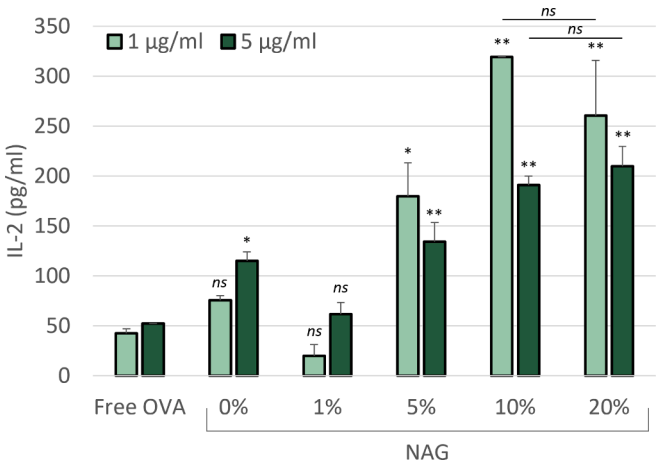

Fig. 5. Antigen specific T cell response. The SIINFEKL-specific B3Z cells were co-cultured with BMDC preincubated with the indicated antigen formulations (NAG prepared with different amounts of DDAB expressed as % on the horizontal axis, or Free OVA) and IL-2 released in cell culture medium was measured by ELISA. Graph is representative of 2 independent experiments, mean ± SD are reported. Symbols indicate statistically significant difference VS Free OVA at the same dose (one-way ANOVA Tukey's multiple comparison test, * $p < 0.05$, **$p < 0.01$, ns not significant).

nanoparticles were administered, probably due to concurrent effects of charge-triggered toxicity.

We speculated that the improved T cell response generated by the nanoparticulate OVA was linked to a higher cell uptake compared to the free protein. OVA, similarly to most soluble antigens, is not efficiently endocytosed and cross-presented by professional APCs and hence is not effective in inducing cell mediated immunity. To confirm our hypothesis, a murine macrophage cell line was exposed for four hours to NAG prepared using a fluorescent OVA conjugate (FITC-OVA). The uninternalized nanoparticles were then washed away, cells were fixed and stained with markers for nuclei and cell membrane and observed by confocal laser scanning microscopy (Fig. 6**, microscopy images)**. Maximum intensity projections of Z stacks allowed to observe bright green fluorescence inside the bodies of cells treated with NAG, confirming the efficient uptake of FITC-OVA when organized as nanoaggregates, irrespective of the amount of cationic lipid employed in the formulation. Conversely, cells treated with an equal amount of soluble FITC-OVA reveal a limited or absent internalization. To gain additional insights into the process, quantitative determination of the intracellular fluorescence was performed by microplate reader following cell lysis to release their content **(**Fig. 6**, histogram)**. The experiment was performed using three different doses of FITC-OVA to better appreciate possible differences between the formulations. At the highest dose (31.25 µg/ml) NAG 20 % showed a 6-fold higher uptake compared to the free FITC-OVA, an observation in agreement with the improvement in antigen-specific T cell response previously discussed. As expected, the ability to being taken up by macrophages was decreased when lower amounts of cationic lipid were included in the formulation. Nevertheless, the quantitative determination confirmed the observation that being organized as a supramolecular nanoaggregate significantly boosts the cell endocytosis, with the minimum improvement shown by NAG 1 % (2.5-fold higher uptake than free FITC-OVA).

3.5. In vivo analysis of immune response to NAG

In order to measure the efficacy of nanoparticulate OVA in inducing cellular response, we injected mice twice subcutaneously at 14 days of distance with an OVA dose of 2.27 mg/kg **(**Fig. 7**A)**. Among the formulations screened in physico-chemical and *in vitro* assays, NAG containing 20 % DDAB (NAG 20 %) was selected for its superior cell uptake

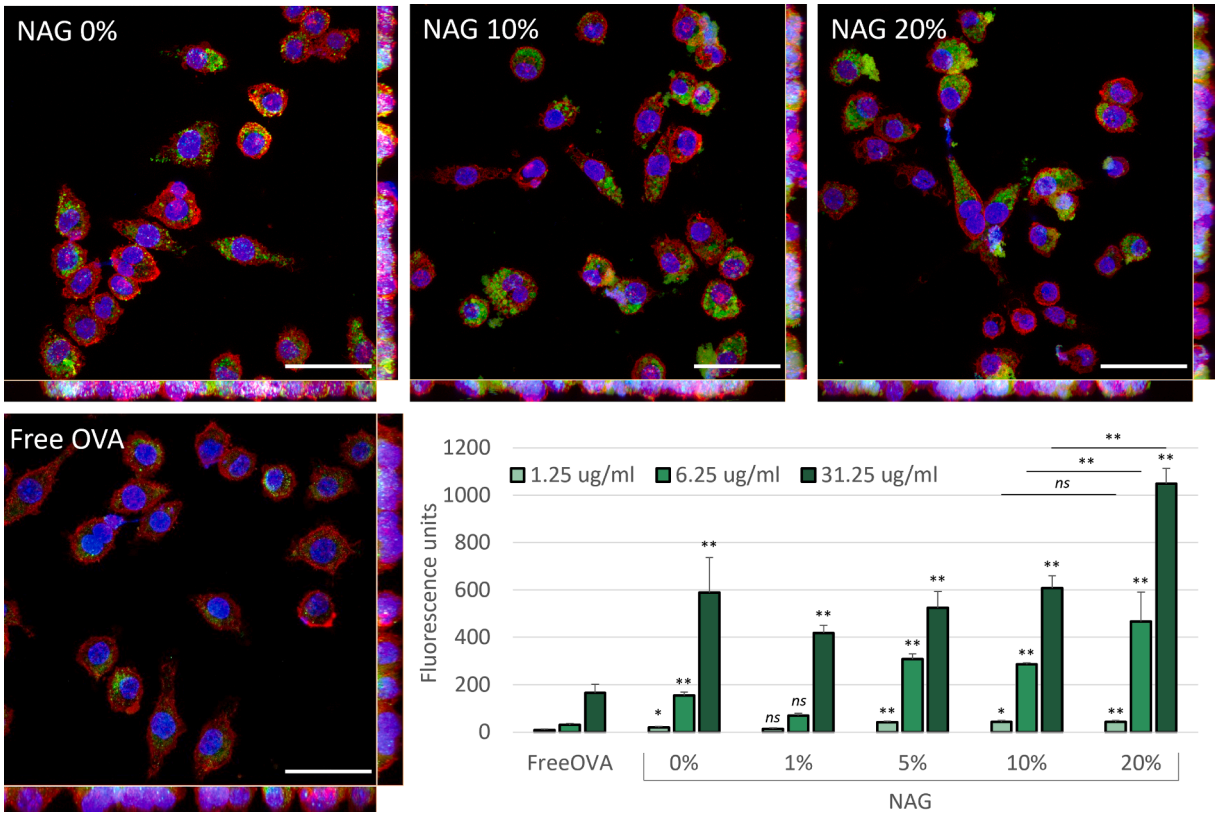

Fig. 6. Uptake of NAG prepared with FITC-OVA by RAW 264.3 cells. Data are shown as confocal microscopy Z-stacks (maximum intensity projections) of cells labeled with DAPI (blue), WGA (red) and treated with FITC-OVA NAG or free FITC-OVA (6.25 μg/ml) (green) prepared with different amounts of cationic surfactant DDAB (expressed as a % on the images). Scalebar = 50 μm. Quantitative data were obtained by measurement of fluorescence by microplate reader, following the lysis of cells treated with FITC-OVA NAG or free FITC-OVA (1.25, 6.25 or 31.25 μg/ml) (n = 6). Symbols indicate statistically significant difference VS Free OVA at the same dose (one-way ANOVA Tukey's multiple comparison test, * $p < 0.05$, **$p < 0.01$, ns not significant).

and ability to induce an antigen-specific T cell response. To mirror vaccine administration, we also adsorbed NAG particles and soluble OVA on alum, an adjuvant licensed for human use. Seven days after boosting, we measured the cellular response as percentage of splenic $CD3^+/CD8^+$ T cells stained by OVA dextramers by cytofluorimetric analysis and appropriate gating strategy **(Supporting** Figure 5**)**. Dextramers are soluble MHC-I molecules loaded with the $OVA_{(257-264)}$ antigen, and selectively bind T cell receptors specific for the $OVA_{(257-264)}$ peptide. As reported in Fig. 7**B**, priming and boosting with NAG induces a significantly higher clonal expansion of OVA-specific T $cells_{(257-264)}$, in comparison to the soluble Ovalbumin. We speculate that this result depends on the efficient NAG antigen uptake by professional antigen presenting cells, while soluble OVA is poorly taken up and cross-presented in MHC-I groove after processing. The alum adjuvant does not induce a significant improvement in antigen-specific T cell expansion.

4. Conclusions

Protein aggregates have a high immunogenic potential, being a concern for the formulation of biopharmaceuticals for chronic therapies. This property has been exploited in the field of vaccine development, where nanoparticulate formulations of protein antigens assembled in different ways –adsorbed on the surface, chemically linked, encapsulated, randomly aggregated- have shown to efficiently activate the adaptive immune response. In this work, we have optimized a method to induce the controlled aggregation of proteins by microfluidic mixing of an antigen aqueous solution with an alcoholic anti-solvent. Lipid-stabilized OVA NAG were obtained, and were able to induce an enhanced antigen-specific T cell response *in vitro* and *in vivo*. Overall, this work provides the proof-of-concept of a quick, robust, and scalable process to produce size-defined aggregates to boost the immunogenic potential of purified protein antigens. Indeed, microfluidic mixing has already shown to be a scalable and robust technique for the production of lipid (Webb et al., 2020) and polymeric nanoparticles (Chiesa et al., 2022). On a different note, the tendency to aggregate when exposed to organic solvent is shared among numerous proteins, with a well-documented underlying mechanism, and a practical use in the downstream processing of antibodies (Yoshikawa et al., 2012). As such, we speculate that the microfluidic method herein described has the potential to be applied to pathogen-derived protein antigens or tumor neo-antigens following a minimal optimization of process parameters.

CRediT authorship contribution statement

Michele Schlich: Writing – review & editing, Writing – original draft, Project administration, Methodology, Investigation, Formal analysis, Data curation, Conceptualization. **Luciana D'Apice:** Writing – original draft, Visualization, Methodology, Investigation, Formal analysis, Data curation. **Francesco Lai:** Visualization, Validation. **Chiara Sinico:** Supervision, Project administration. **Donatella Valenti:** Methodology. **Federico Catalano:** Visualization, Methodology, Investigation. **Roberto Marotta:** Methodology, Investigation. **Paolo Decuzzi:** Writing – review & editing, Supervision, Resources. **Paola Italiani:** Writing – original draft, Resources, Investigation, Funding acquisition, Formal analysis. **Anna Maria Fadda:** Writing – review & editing, Supervision, Resources, Project administration, Funding acquisition.

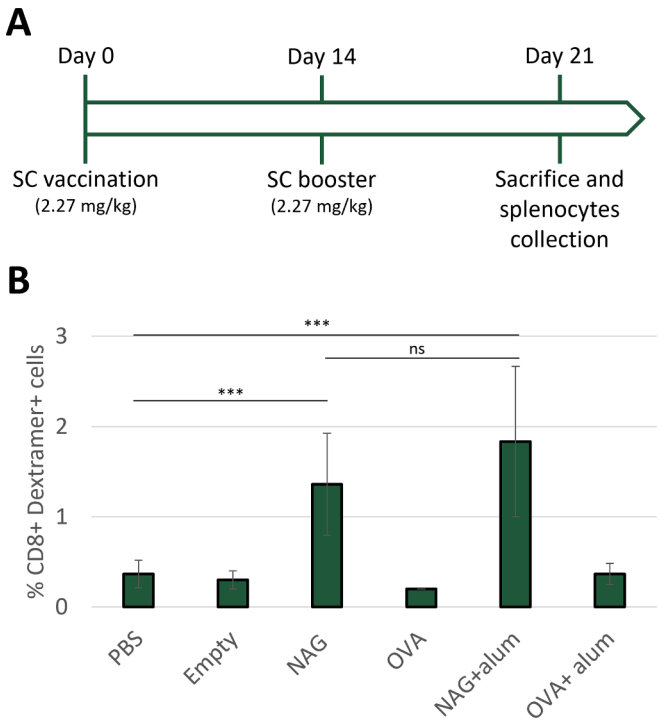

Fig. 7. Schematic representation of vaccination schedule (SC, sub-cutaneous) (**A**). C57Bl/6 mice (n = 3/6) were subcutaneously injected at day 0 and day 14 with indicated compounds (2.27 mg_{OVA}/kg). At day 21 mice were sacrificed and splenocytes were collected and stained for FACS analysis. (**B**) Percentage of $OVA_{(257-264)}$ specific $CD8^+$ T cells were measured by FACS analysis on $CD3^+$/$CD8^+$ gated cells. Mean ± SD are reported. Symbols indicate statistically significant difference between treatments (one-way ANOVA Tukey's multiple comparison test, *** $p < 0.005$, ns not significant).

Declaration of competing interest

The authors declare that they have no known competing financial interests or personal relationships that could have appeared to influence the work reported in this paper.

Data availability

Data will be made available on request.

Acknowledgments

This work was supported by the following grants: Project PRIN 2017, n. 20173ZECCM, "Tackling biological barriers to antigen delivery by nanotechnological vaccines (NanoTechVax)", funded by Italian Ministry of University and Research; Project PON ARS01_00906 "TITAN - Nanotecnologie per l'immunoterapia dei tumori", funded by the Italian FESR-PON Research and Innovation. MS acknowledge the support by EU FSE-REACT PON Research and Innovation 2014–2020 (DM1062/2021). The authors acknowledge the CeSAR core facility of the University of Cagliari and Dr. Giulio Ferino for assistance with LC/MS experiments.

Appendix A. Supplementary data

Supplementary data to this article can be found online at https://doi.org/10.1016/j.ijpharm.2024.124404.

Bibliography

Ahmad, F., Zubair, S., Gupta, P., Gupta, U.D., Patel, R., Owais, M., 2017. Evaluation of aggregated Ag85B antigen for its biophysical properties, immunogenicity, and vaccination potential in a murine model of tuberculosis infection. Front. Immunol. 8 https://doi.org/10.3389/fimmu.2017.01608.

Blass, E., Ott, P.A., 2021. Advances in the development of personalized neoantigen-based therapeutic cancer vaccines. Nat. Rev. Clin. Oncol. 18, 215–229. https://doi.org/10.1038/s41571-020-00460-2.

Carson, C.S., Becker, K.W., Garland, K.M., Pagendarm, H.M., Stone, P.T., Arora, K., Wang-Bishop, L., Baljon, J.J., Cruz, L.D., Joyce, S., Wilson, J.T., 2022. A nanovaccine for enhancing cellular immunity via cytosolic co-delivery of antigen and polyIC RNA. J. Control. Release 345, 354–370. https://doi.org/10.1016/j.jconrel.2022.03.020.

Chatzikleanthous, D., Schmidt, S.T., Buffi, G., Paciello, I., Cunliffe, R., Carboni, F., Romano, M.R., O'Hagan, D.T., D'Oro, U., Woods, S., Roberts, C.W., Perrie, Y., Adamo, R., 2020. Design of a novel vaccine nanotechnology-based delivery system comprising CpGODN-protein conjugate anchored to liposomes. J. Control. Release 323, 125–137. https://doi.org/10.1016/j.jconrel.2020.04.001.

Chiesa, E., Bellotti, M., Caimi, A., Conti, B., Dorati, R., Conti, M., Genta, I., Auricchio, F., 2022. Development and optimization of microfluidic assisted manufacturing process to produce PLGA nanoparticles. Int. J. Pharm. 629, 122368 https://doi.org/10.1016/j.ijpharm.2022.122368.

Collins, D.R., Gaiha, G.D., Walker, B.D., 2020. CD8+ T cells in HIV control, cure and prevention. Nat. Rev. Immunol. 20, 471–482. https://doi.org/10.1038/s41577-020-0274-9.

Dong, X., Sun, Z., Liang, J., Wang, H., Zhu, D., Leng, X., Wang, C., Kong, D., Lv, F., 2018. A visible fluorescent nanovaccine based on functional genipin crosslinked ovalbumin protein nanoparticles. Nanomedicine Nanotechnology. Biol. Med. 14, 1087–1098. https://doi.org/10.1016/j.nano.2018.02.007.

Foged, C., Hansen, J., Agger, E.M., 2012. License to kill: Formulation requirements for optimal priming of CD8 + CTL responses with particulate vaccine delivery systems. Eur. J. Pharm. Sci. 45, 482–491. https://doi.org/10.1016/j.ejps.2011.08.016.

Forbes, N., Hussain, M.T., Briuglia, M.L., Edwards, D.P., te Horst, J.H., Szita, N., Perrie, Y., 2019. Rapid and scale-independent microfluidic manufacture of liposomes entrapping protein incorporating in-line purification and at-line size monitoring. Int. J. Pharm. 556, 68–81. https://doi.org/10.1016/j.ijpharm.2018.11.060.

Gao, J., Ochyl, L.J., Yang, E., Moon, J.J., 2017. Cationic liposomes promote antigen cross-presentation in dendritic cells by alkalizing the lysosomal pH and limiting the degradation of antigens. Int. J. Nanomedicine 12, 1251–1264. https://doi.org/10.2147/IJN.S125866.

Hawe, A., Kasper, J.C., Friess, W., Jiskoot, W., 2009. Structural properties of monoclonal antibody aggregates induced by freeze-thawing and thermal stress. Eur. J. Pharm. Sci. 38, 79–87. https://doi.org/10.1016/j.ejps.2009.06.001.

Jiang, W., Pilkington, E.H., Kelly, H.G., Tan, H.X., Juno, J.A., Wheatley, A.K., Kent, S.J., 2020. Aggregation by peptide conjugation rescues poor immunogenicity of the HA stem. PLoS One 15, 1–15. https://doi.org/10.1371/journal.pone.0241649.

Kapadia, C.H., Tian, S., Perry, J.L., Luft, J.C., Desimone, J.M., 2016. Reduction sensitive PEG hydrogels for codelivery of antigen and adjuvant to induce potent CTLs. Mol. Pharm. 13, 3381–3394. https://doi.org/10.1021/acs.molpharmaceut.6b00288.

Khadke, S., Roces, C.B., Cameron, A., Devitt, A., Perrie, Y., 2019. Formulation and manufacturing of lymphatic targeting liposomes using microfluidics. J. Control. Release 307, 211–220. https://doi.org/10.1016/j.jconrel.2019.06.002.

Kim, K.S., Lee, S., Na, K., Bae, Y.H., 2022. Ovalbumin and poly(i:c) encapsulated dendritic cell-targeted nanoparticles for immune activation in the small intestinal lymphatic system. Adv. Healthc. Mater. 11, 1–11. https://doi.org/10.1002/adhm.202200909.

Knudsen, K.B., Northeved, H., Pramod Kumar, E.K., Permin, A., Gjetting, T., Andresen, T. L., Larsen, S., Wegener, K.M., Lykkesfeldt, J., Jantzen, K., Loft, S., Møller, P., Roursgaard, M., 2015. In vivo toxicity of cationic micelles and liposomes. Nanomedicine Nanotechnology. Biol. Med. 11, 467–477. https://doi.org/10.1016/j.nano.2014.08.004.

Könnings, S., Copland, M.J., Davies, N.M., Rades, T., 2002. A method for the incorporation of ovalbumin into immune stimulating complexes prepared by the hydration method. Int. J. Pharm. 241, 385–389. https://doi.org/10.1016/S0378-5173(02)00270-3.

Ma, Y., Zhuang, Y., Xie, X., Wang, C., Wang, F., Zhou, D., Zeng, J., Cai, L., 2011. The role of surface charge density in cationic liposome-promoted dendritic cell maturation and vaccine-induced immune responses. Nanoscale 3, 2307–2314. https://doi.org/10.1039/c1nr10166h.

Nguyen, B., Tolia, N.H., 2021. Protein-based antigen presentation platforms for nanoparticle vaccines. npj Vaccines 6. https://doi.org/10.1038/s41541-021-00330-7.

Pati, R., Shevtsov, M., Sonawane, A., 2018. Nanoparticle vaccines against infectious diseases. Front. Immunol. 9 https://doi.org/10.3389/fimmu.2018.02224.

Pedersen, G.K., Andersen, P., Christensen, D., 2018. Immunocorrelates of CAF family adjuvants. Semin. Immunol. 39, 4–13. https://doi.org/10.1016/j.smim.2018.10.003.

Pollard, A.J., Bijker, E.M., 2020. A guide to vaccinology: from basic principles to new developments. Nat. Rev. Immunol. https://doi.org/10.1038/s41577-020-00479-7.

Rupa, P., Mine, Y., 2011. Egg proteins. Handbook of Food Proteins. 150–209. https://doi.org/10.1533/9780857093639.150.

Sartorius, R., D'Apice, L., Barba, P., Cipria, D., Grauso, L., Cutignano, A., De Berardinis, P., 2018. Vectorized delivery of alpha-Galactosylceramide and tumor antigen on filamentous bacteriophage fd induces protective immunity by enhancing tumor-specific T cell response. Front. Immunol. 9, 1–13. https://doi.org/10.3389/fimmu.2018.01496.

Schmidt, S.T., Khadke, S., Korsholm, K.S., Perrie, Y., Rades, T., Andersen, P., Foged, C., Christensen, D., 2016. The administration route is decisive for the ability of the vaccine adjuvant CAF09 to induce antigen-specific CD8+ T-cell responses: The

immunological consequences of the biodistribution profile. J. Control. Release 239, 107–117. https://doi.org/10.1016/j.jconrel.2016.08.034.
Seder, R.A., Darrah, P.A., Roederer, M., 2008. T-cell quality in memory and protection: Implications for vaccine design. Nat. Rev. Immunol. 8, 247–258. https://doi.org/10.1038/nri2274.
Shimp, R.L., Rowe, C., Reiter, K., Chen, B., Nguyen, V., Aebig, J., Rausch, K.M., Kumar, K., Wu, Y., Jin, A.J., Jones, D.S., Narum, D.L., 2013. Development of a Pfs25-EPA malaria transmission blocking vaccine as a chemically conjugated nanoparticle. Vaccine 31, 2954–2962. https://doi.org/10.1016/j.vaccine.2013.04.034.
Snapper, C.M., 2018. Distinct immunologic properties of soluble versus particulate antigens. Front. Immunol. 9 https://doi.org/10.3389/fimmu.2018.00598.
Speidel, K., Faath, S., Hilged, I., Obst, R., Braspenning, J., Mombu, F., Hammerlings, G.J., 1997. Priming of cytotoxic T lymphocytes by five heat- aggregated antigens in vivo : conditions, efficiency. Eur. J. Immunol. 27, 2391–2399.
Tabassum, M., Tiboni, M., Perrie, Y., Casettari, L., 2020. Microfluidic production of protein loaded chimeric stealth liposomes. Int. J. Pharm. 590, 119955 https://doi.org/10.1016/j.ijpharm.2020.119955.
Tian, J.H., Patel, N., Haupt, R., Zhou, H., Weston, S., Hammond, H., Logue, J., Portnoff, A.D., Norton, J., Guebre-Xabier, M., Zhou, B., Jacobson, K., Maciejewski, S., Khatoon, R., Wisniewska, M., Moffitt, W., Kluepfel-Stahl, S., Ekechukwu, B., Papin, J., Boddapati, S., Jason Wong, C., Piedra, P.A., Frieman, M.B., Massare, M.J., Fries, L., Bengtsson, K.L., Stertman, L., Ellingsworth, L., Glenn, G., Smith, G., 2021. SARS-CoV-2 spike glycoprotein vaccine candidate NVX-CoV2373 immunogenicity in baboons and protection in mice. Nat. Commun. 12 https://doi.org/10.1038/s41467-020-20653-8.
Urbanavicius, D., Alvarez, T., Such, G.K., Johnston, A.P.R., Mintern, J.D., 2018. The potential of nanoparticle vaccines as a treatment for cancer. Mol. Immunol. 98, 2–7. https://doi.org/10.1016/j.molimm.2017.12.022.
Van Duin, D., Medzhitov, R., Shaw, A.C., 2006. Triggering TLR signaling in vaccination. Trends Immunol. 27, 49–55. https://doi.org/10.1016/j.it.2005.11.005.
van Oss, C.J., 1989. On the mechanism of the cold ethanol precipitation method of plasma protein fractionation. J. Protein Chem. 8, 661–668. https://doi.org/10.1007/BF01025606.
Varypataki, E.M., Silva, A.L., Barnier-Quer, C., Collin, N., Ossendorp, F., Jiskoot, W., 2016. Synthetic long peptide-based vaccine formulations for induction of cell mediated immunity: A comparative study of cationic liposomes and PLGA nanoparticles. J. Control. Release 226, 98–106. https://doi.org/10.1016/j.jconrel.2016.02.018.
Walls, A.C., Fiala, B., Schäfer, A., Wrenn, S., Pham, M.N., Murphy, M., Tse, L.V., Shehata, L., O'Connor, M.A., Chen, C., Navarro, M.J., Miranda, M.C., Pettie, D., Ravichandran, R., Kraft, J.C., Ogohara, C., Palser, A., Chalk, S., Lee, E.C., Guerriero, K., Kepl, E., Chow, C.M., Sydeman, C., Hodge, E.A., Brown, B., Fuller, J. T., Dinnon, K.H., Gralinski, L.E., Leist, S.R., Gully, K.L., Lewis, T.B., Guttman, M., Chu, H.Y., Lee, K.K., Fuller, D.H., Baric, R.S., Kellam, P., Carter, L., Pepper, M., Sheahan, T.P., Veesler, D., King, N.P., 2020. Elicitation of potent neutralizing antibody responses by designed protein nanoparticle vaccines for SARS-CoV-2. Cell 183, 1367–1382.e17. https://doi.org/10.1016/j.cell.2020.10.043.
Wang, C., Liu, P., Zhuang, Y., Li, P., Jiang, B., Pan, H., Liu, L., Cai, L., Ma, Y., 2014. Lymphatic-targeted cationic liposomes: A robust vaccine adjuvant for promoting long-term immunological memory. Vaccine 32, 5475–5483. https://doi.org/10.1016/j.vaccine.2014.07.081.
Wang, W., Singh, S.K., Li, N., Toler, M.R., King, K.R., Nema, S., 2012. Immunogenicity of protein aggregates - Concerns and realities. Int. J. Pharm. 431, 1–11. https://doi.org/10.1016/j.ijpharm.2012.04.040.
Webb, C., Forbes, N., Roces, C.B., Anderluzzi, G., Lou, G., Abraham, S., Ingalls, L., Ingalls, L., Marshall, K., Leaver, T.J., Watts, J.A., Aylott, J.W., Perrie, Y., 2020. Using microfluidics for scalable manufacturing of nanomedicines from bench to GMP: A case study using protein-loaded liposomes. Int. J. Pharm. 582, 119266 https://doi.org/10.1016/j.ijpharm.2020.119266.
Wei, X., Shao, B., He, Z., Ye, T., Luo, M., Sang, Y., Liang, X., Wang, W., Luo, S., Yang, S., Zhang, S., Gong, C., Gou, M., Deng, H., Zhao, Y., Yang, H., Deng, S., Zhao, C., Yang, L., Qian, Z., Li, J., Sun, X., Han, J., Jiang, C., Wu, M., Zhang, Z., 2015. Cationic nanocarriers induce cell necrosis through impairment of Na+/K+-ATPase and cause subsequent inflammatory response. Cell Res. 25, 237–253. https://doi.org/10.1038/cr.2015.9.
White, P.J., Anastasopoulos, F., Church, J.E., Kuo, C.Y., Boyd, B.J., Hickey, P.L.C., Tu, L. S., Burns, P., Lew, A.M., Heath, W.R., Davey, G.M., Pouton, C.W., 2008. Generic construction of single component particles that elicit humoural and cellular immune responses without the need for adjuvants. Vaccine 26, 6824–6831. https://doi.org/10.1016/j.vaccine.2008.09.087.
White, P.J., Hickey, P., Sze Tu, L., Headey, S.J., Scanlon, M.J., Boyd, B.J., Pouton, C.W., 2012. Colloidal characteristics and formulation of pure protein particulate vaccines. J. Pharm. Pharmacol. 64, 1386–1393. https://doi.org/10.1111/j.2042-7158.2012.01513.x.
Yoshikawa, H., Hirano, A., Arakawa, T., Shiraki, K., 2012. Mechanistic insights into protein precipitation by alcohol. Int. J. Biol. Macromol. 50, 865–871. https://doi.org/10.1016/j.ijbiomac.2011.11.005.